Molecular Crystals and Liquid Crystals

ISSN: (Print) (Online) Journal homepage: www.tandfonline.com/journals/gmcl20

Investigation of nano-rods fabricated by the DNA origami method using static and dynamic light scattering

Bingru Zhang, Kevin Martens, Luisa Kneer, Linh Nguyen, Susanne Kempter, Klaus Huber & Heinz-S. Kitzerow

To cite this article: Bingru Zhang, Kevin Martens, Luisa Kneer, Linh Nguyen, Susanne Kempter, Klaus Huber & Heinz-S. Kitzerow (2025) Investigation of nano-rods fabricated by the DNA origami method using static and dynamic light scattering, Molecular Crystals and Liquid Crystals, 769:1, 1-9, DOI: 10.1080/15421406.2024.2418067

To link to this article: https://doi.org/10.1080/15421406.2024.2418067

MOLECULAR CRYSTALS AND LIQUID CRYSTALS
2025, VOL. 769, NO. 1, 1–9
https://doi.org/10.1080/15421406.2024.2418067

Taylor & Francis
Taylor & Francis Group

Investigation of nano-rods fabricated by the DNA origami method using static and dynamic light scattering

Bingru Zhang[a], Kevin Martens[b], Luisa Kneer[b], Linh Nguyen[b], Susanne Kempter[b], Klaus Huber[a], and Heinz-S. Kitzerow[a]

[a]Paderborn University, Paderborn, Germany; [b]Department of Physics, Ludwig-Maximilians-Universität, München, Germany

ABSTRACT

Dilute aqueous dispersions of rod-like DNA helix bundles prepared by the DNA origami method are studied using static and dynamic light scattering. Observed masses and sizes of the scattering particles agree in principle with the properties that are expected. Only the ratio of the radius of gyration and the hydrodynamic radius deviates from the expectation for rigid rods for some samples, seemingly indicating a more coil-like behavior. To which extent this observation might be attributed to a hindered rotational and translational diffusion caused by unpaired single stranded DNA sections remains to be investigated.

KEYWORDS

DNA origami; light scattering; nano-particles

1. Introduction

The polyelectrolyte deoxyribonucleic acid (DNA) is not only known to carry genetic information, it is also an extremely versatile liquid crystal (LC) component. Aqueous solutions of DNA can form lyotropic LCs [1, 2], DNA and DNA-surfactant complexes appear in thermotropic LCs [3], and DNA nanoparticles fabricated using the tailored folding of DNA ('DNA origami') can act as building blocks for colloidal LCs [4]. Even the origin of life may have been supported by the self-assembly of short DNA strands to larger aggregates [5]. In addition, mutual aligning effects of lyotropic and thermotropic LCs [6, 7], the influence of anisometric colloidal DNA nanoparticles on a lyotropic chromonic liquid crystal [8, 9] and the optical effects of switchable chirality of plasmonic DNA nanoparticles dispersed in a lyotropic LC [10] have been studied. This work is focused on light scattering investigations of dilute solutions of DNA nanoparticles which are fabricated by the DNA origami technique.

DNA Origami is a high-performing method of fabricating nanoparticles with precisely defined size, shape and functionality [11–16]. The technique is based on folding DNA into monomolecular sheets [17], three-dimensional nanostructures [18] and larger

CONTACT Heinz-S. Kitzerow Heinz.Kitzerow@upb.de Paderborn University, Paderborn 33098, Germany.
Supplemental data for this article can be accessed online at https://doi.org/10.1080/15421406.2024.2418067.

assemblies made thereof [19]. Additional attachment of functional molecular moieties or nanoparticles facilitates versatile applications, for example, in metrology, optics and photonics, organic electronics, sensing or diagnostics. Typically, a single-stranded DNA macromolecule ('scaffold' with ≈ 7000-8000 nucleotides) obtained from a natural bacteriophage virus is mixed with about 100 to 200 single-stranded DNA oligomers ('staples', ≈ 30-40 nucleotides each). An individual staple attaches to two specific locations on the scaffold, thereby directing its folding process and resulting in a precisely defined final shape of the generated nanoparticles [20–24]. The accuracy of the nanostructure formation is governed by the spacing between neighboring nucleotides (≈ 0.34 nm), the diameter of the DNA double helix (≈ 2 nm), and the helix pitch (≈ 10.5 nucleotide spacings) [25, 26]. Computer-aided design is utilized to determine the required staple sequences for achieving the desired shape of the resulting nanoparticles [20–24]. In the present study, cylindrical particles with varying aspect ratio (length/width) [27] were fabricated and characterized using static and dynamic light scattering. Small angle X-ray scattering [25, 28] and light scattering [29] have been used previously to study the structure of pure [25] or silica-stabilized [28] DNA origami particles and the dynamics of their assembly or enzymatic degradation [29], respectively. Here, we focus on the investigation of molar mass, radius of gyration, translational diffusion constant and hydrodynamic radius of DNA origami nano-rods by means of static and dynamic light scattering.

2. Experiments: DNA nano-rod synthesis, purification, and light scattering studies

The synthesis followed standard DNA origami procedures. A mixture of the single-stranded DNA scaffold and 196 to 227 single-stranded DNA staples was prepared in an alkaline buffer solution ("Rotistock", Carl Roth) containing 14-18 mM magnesium chloride ($MgCl_2$). The mixture was heated to 65 °C and then slowly cooled to room temperature over 25 h, allowing for folding. During the folding process, Mg^{2+} cations of $MgCl_2$ effectively compensated for the repulsive interaction of negative charges from phosphate groups in the DNA. In the present study, DNA nano-rods were prepared, which consist of bundles of 24, 18 and 14 of double-stranded DNA helices, referred to as 24-helix bundle (24HB), 18-helix bundle (18HB), and 14-helix bundle (14HB), respectively. Details of the protocol can be found in Table 1, while the precise designs of the DNA origami structures (tailored using caDNAno and CanDo software) are shown in Figs. S1 to S5 in the Supporting Information. In addition to the staples, the cylindrical nanoparticles bear lateral single stranded oligonucleotides ('handles', with a length of 19 nucleotides each) for the purpose of potential functionalization with nanoparticles to be added.

Table 1. Synthesis details for DNA origami nano-rods.

Design	No. of nucleotides of the scaffold	No. of staples	Excess of staple concentration	Cooling duration of folding (h)	Buffer	Concentration of $MgCl_2$ (mM)
24HB	7560	210	10×	25.3	TE	14
18HB	7560	196	10×	25.3	TE	18
14HB	8634	227	3×	24.6	TE	18

Table 2. Theoretical and experimental dimensions of DNA origami nano-rods with 24-helix bundles (24HB), 18-helix bundles (18HB), and 14-helix bundles (14HB).

Design	L_{theo} [nm]	L_{exp} [nm]	D_{th} [nm]	D_{exp} [nm]
24HB	107.10	108.5 ± 3.1	16.76	12.3 ± 0.5
18HB	142.80	132.5 ± 3.7	13.60	11.8 ± 1.4
14HB	209.68	204.6 ± 10.3	11.00	11.8 ± 1.2

The experimental values are derived from TEM and AFM observations.

After being assembled, the origami nano-rods were purified through spin filtration (Amicon Ultra 0.5 mL, Ultracel 100K, Merck) and washing with 11 mM $MgCl_2$ – 1x TE buffer to eliminate excess staple strands. The purified DNA was then analyzed using either transmission electron microscopy (TEM, model JEM-1011, JEOL) or atomic force microscopy (AFM, Bruker Dimension Icon PT). Since scaffolds exhibiting similar numbers of nucleotides were used to assemble the nHB particles (with $n = 24$, 18 and 14), the theoretical diameter D_{th} of the nano-rods increases, while their theoretical length L_{th} decreases with increasing number n of parallel double helices in the bundle (Table 2). This expectation is confirmed by the respective experimental values of the diameter D_{exp} and the length L_{exp} observed in AFM and TEM experiments.

The angular dependence of light scattering intensity was measured using an ALV/CGS-3 MD-8 goniometer system equipped with a HeNe laser ($\lambda = 632$ nm) and analyzed as explained in the Supporting Information [Equations (SI-1) to (SI-6)].

3. Results

3.1. Static light scattering

Preliminary static scattering (SLS) experiments of DNA Origami at concentrations beyond a certain limit which depends on the specific Origami sample revealed strongly bent scattering curves pointing to unexpectedly large radii of gyration and molar mass values more than an order of magnitude larger than expected on grounds of theoretical estimations. Most likely, self-assembly of the DNA Origami particles interfered with an interpretation of the SLS data in terms of single particle properties, forcing us to lower the highest concentration as far as possible yet still providing acceptable signal to noise ratios. Accordingly, the highest concentrations analyzed were 15.21 nM (14HB), 1.09 nM (18HB) and 5.78 nM (24HB).

The results of these SLS data, represented as Zimm-plots [30] are shown in Fig. S6 in the Supporting Information. The apparent molar mass and the apparent radius of gyration derived from the intercept and the q-dependent slope at variable c are shown in Fig. 1.

Extrapolation of the apparent values to $c = 0$ (Fig. 1 and Fig. S6) yields the following molar mass values $M_{w,\exp}$: 4.7×10^6 g/mol for 24HB, 4.8×10^6 g/mol for 18HB, and 3.5×10^6 g/mol for 14HB. These experimental findings are compared with theoretical data denoted as $M_{w,theo}$ and $R_{g,theo}$ in Table 3. Theoretical values were calculated by means of the size of the scaffold and the number of staples shown in Table 2. Except for sample 14HB, where the experimental value $M_{w,\exp}$ is significantly lower than the theoretical value of $M_{w,theo}$, agreement is considered to be very good in the light of the experimental uncertainty caused by the low concentrations analyzed and by the

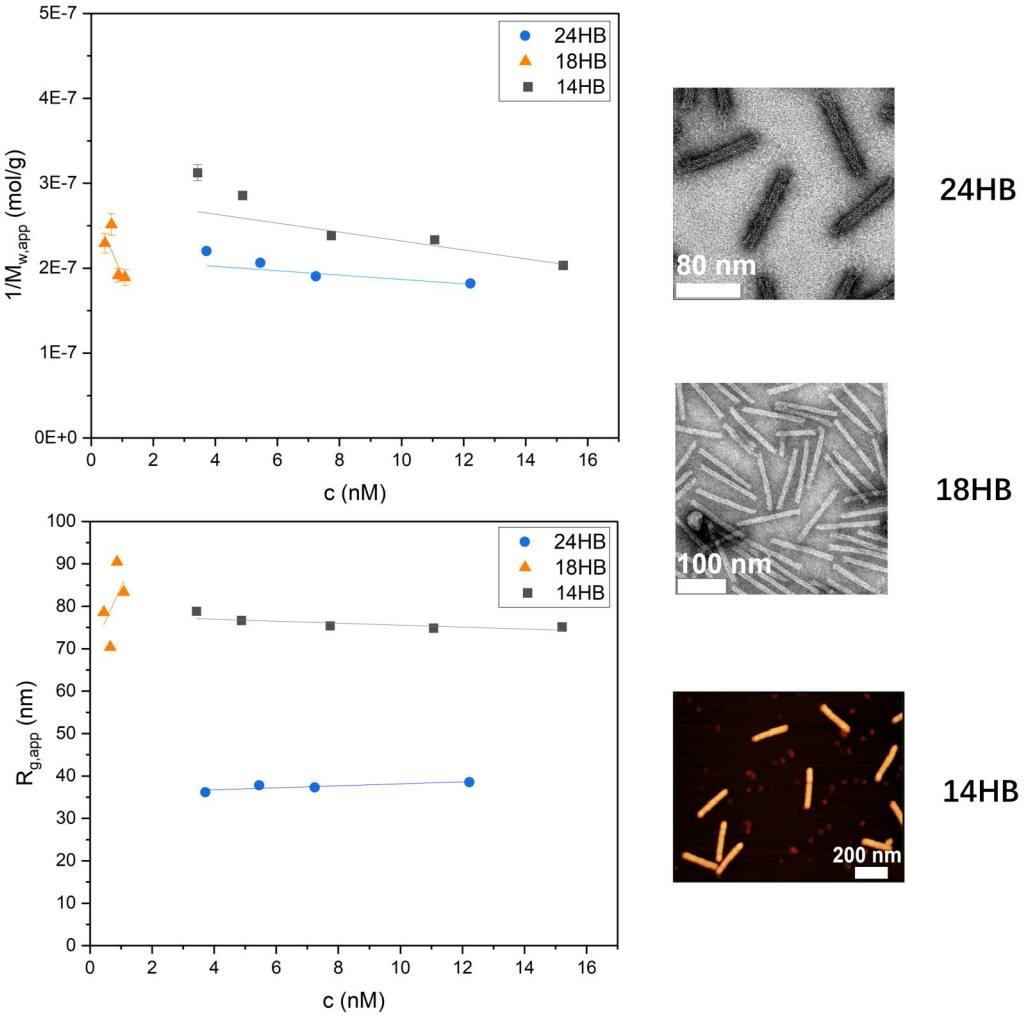

Figure 1. Concentration dependence of the inverse apparent weight averaged molar mass $M_{w,app}$ and of the apparent radius of gyration $R_{g,app}$ derived from Zimm-plots [30] for origami nano-rods of samples 24HB, 18HB, and 14HB (to the left), and images obtained by transmission electron microscopy (24HB and 18HB) or atomic force microscopy (14HB) showing these origami nano-rods (to the right).

Table 3. Weight-average molar masses and square root of the z-averaged squared radius of gyration from SLS of 24HB, 18HB, and 14HB.

SLS data	24HB	18HB	14HB
$R_{g,exp}$ [nm]	35.8	80.1	77.9
L_{SLS} [nm]	124	277	270
L_{theo} [nm]	107.10	142.80	209.68
$M_{w,exp}$ [g/mol]	$(4.7 \pm 0.3) \times 10^6$	$(4.8 \pm 1.0) \times 10^6$	$(3.5 \pm 1.5) \times 10^6$
$M_{w,theo}$ [g/mol]	4.59×10^6	4.59×10^6	5.24×10^6

Rod lengths are calculated with Equation (1). Theoretical values are based on data from Table 1.

additional uncertainty introduced by dn/dc entering data evaluation as squared value [Equation (SI-3) in the Supporting Information]. Only sample 14HB shows an unexpectedly high deviation between theory and experiment.

An experimental value which is 30% lower than expected was observed for sample 14HB and might be caused by a loss of some material during sample preparation. Additionally, only part of the staples may have been bound to the scaffold in the folding mixture of 14HB, where the concentration of the staples exceeded the concentration of the scaffold only by a factor of three (as opposed to a factor of 10 in the folding mixtures of 24HB and 18HB, see Table 1 and Supporting Information, page 5). On the other hand, AFM confirms the proper shape expected for the 14HB particles (Fig. 1).

Turning to the radius of gyration as the geometric size value inferred from SLS, a similar comparison can be performed. Given, that the DNA origami particles adopt rod-like structures and that the samples are monodisperse, a rod length can be derived from the radius of gyration by utilizing the formula

$$L_{SLS} = \sqrt{12 \cdot {R_{g,\exp}}^2} \tag{1}$$

The resulting lengths are summarized in Table 3 and can be compared with the respective theoretical values given in Table 2. The values extracted from microscopic images are also included in Table 2 being in good agreement with the theoretically predicted values (2nd and 3rd column in Table 2). If length values from SLS are compared with those from microscopy, again two samples, now 14HB and 24HB, exhibit fair agreement given the difference of such techniques. A small shrinking is likely to occur in the dried state of substrates used for microscopy and might explain the slightly smaller values observed in microscopic images. Only in case of sample 18HB do we observe a large discrepancy, which is difficult to explain.

Taken together SLS data from sample 24HB shows best agreement with theoretically expected values, both with respect to the length of the particles as well as with the mass of the particles.

One hypothesis regarding the deviation of molecular weight (M_w) and length (L) from their theoretical values is the potential detachment of certain shorter staple strands from the scaffold strands within the folded origami structure. This detachment might occur due to interactions during the filtration process, causing a shift from the initially compact structure to a more relaxed state and consequently resulting in an overall increase in the length. These alterations contribute to a reduction in the weight-average molecular weight (M_w) while enhancing the length (L).

To assess the structural integrity of the DNA origami sample before and after filtration, we examined the example of 18HB using atomic force microscopy (AFM). The AFM image (Fig. 2) shows that the structure and size of the 18HB origami nano-rods remained largely unchanged after filtration. This result indicates that the filtration process did not affect the integrity of the folded structure.

3.2. Dynamic light scattering

Dynamic light scattering (DLS) yields the translational diffusion coefficient D_0 (Figs. 3 and 4, Table 4) and the hydrodynamic radius $R_{h,exp}$ (Table 5) using standard procedures, as explained in the Supporting Information.

In case of sample 18HB the highly diluted solutions produce large signal to noise ratios, which generate a larger uncertainty in the resulting apparent diffusion

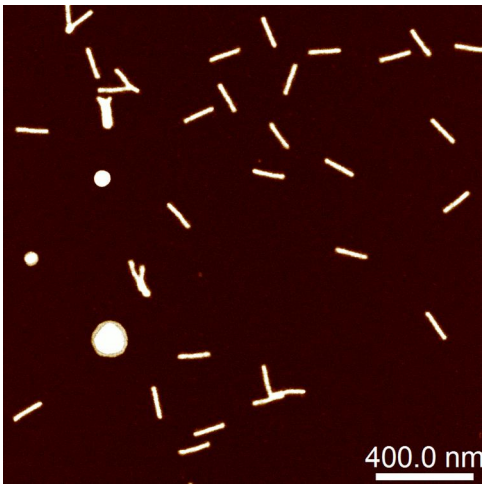

Figure 2. AFM image of the 18HB Structure after filtration. The observed length measures 137 nm. Notably, these measurements remain consistent with the pre-filtration dimensions (Fig. 1, Table 2).

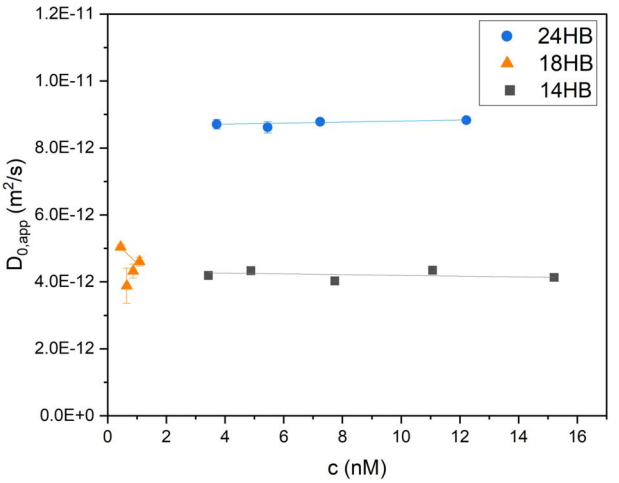

Figure 3. The apparent diffusion coefficient as a function of DNA concentration for 14HB (black squares), 18HB (red triangles), and 24HB (blue spheres). Extrapolation to $c = 0$ reveals D_0, which can be used to calculate the hydrodynamically effective radius according to Equation (SI-4).

Table 4. The values of D_0 for 24HB, 18HB, and 14HB, respectively.

	24HB	18HB	14HB
D_0 [m^2/s]	8.65×10^{-12}	5.38×10^{-12}	4.31×10^{-12}

Table 5. Hydrodynamic radii of cylindrical nano-rods measured via DLS and respective shape sensitive ratios ρ calculated from experimentally derived radius of gyration R_g and hydrodynamic radius R_h according to Equation (2).

Quantity	Symbol	24HB	18HB	14HB
Hydrodynamic radius	$R_{h,exp.}$ [nm]	28.41	54.16	58.12
Shape Sensitive ratio	ρ ($R_{g,exp}$ /$R_{h,exp}$)	2.74	1.48	1.34

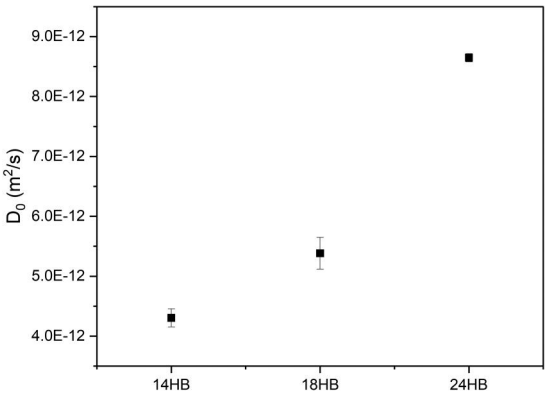

Figure 4. Translational diffusion coefficients extracted from data in Figure 3 via extrapolation to $c = 0$.

coefficients. The values of D_0 obtained at variable concentrations for both 24HB and 14HB show little change. As the concentration increases, D_0 for 24HB increases slightly, while in contrast, D_0 for 14HB decreases slightly (Fig. 3). Accordingly, limits representing the state at infinite dilution were either averaged (18HB) or extrapolated to $c = 0$ (14HB and 24HB) and summarized in Fig. 4 and Table 4. It is evident that as the rod-like structure becomes longer, its translational diffusion coefficient D_0 decreases.

Using the Stokes-Einstein relation [Equation (SI-4) in the Supporting Information], D_0 is translated into the hydrodynamic radius $R_{h,exp}$ (Table 5). The hydrodynamic radius is the radius of an equivalent sphere exhibiting the same translational diffusion coefficient as the particle under consideration. Accordingly, structural information can be extracted from a comparison of the radius of gyration as a geometrical parameter with the corresponding hydrodynamically effective radius. The ratio of the two radii

$$\rho = \frac{R_g}{R_h} \tag{2}$$

is sensitive to the shape of the particles. For spheres [31], a value of 0.78 is predicted, for flexible polymer coils [31], the ratio adopts values between 1.3 and 1.5, and for thin rod-like particles [32], the value gets larger than 2. As is shown in Table 5, the values are significantly larger than those for spheres but samples 14HB and 18HB are far from reaching values typical for thin rod-like particles. Strikingly it is sample 24HB which already showed SLS data fully consistent with the anticipated rods, which also reveals a value for the ρ-ratio typical for rods.

4. Conclusions

Static and dynamic light scattering experiments validate the structure of the DNA nano-rods and fully confirm the anticipated properties in the case of 24HB. The observed molecular weights M_w of sample 14HB was lower by 30% than expected, suggesting that not all staples may have interacted with the scaffold. The radius of gyration R_g and hydrodynamic radius R_h both increase as the length L of the nano-rods grows $L_{14HB} > L_{18HB} > L_{24HB}$. Remarkably, the ratio $\rho = R_{g,\,\mathrm{exp.}}/R_{h,\,\mathrm{exp.}}$, which is anticipated to be

larger than two for rod-like particles, deviates significantly from this expectation in case of 14HB and 18HB and aligns more closely with the value anticipated for random coils ($\rho = 1.33$). In principle, a behavior similar to random coils could be expected if the persistence length of the particles would be rather small. However, former systematic studies of the persistence length of nano-rods fabricated by the DNA origami method [33] confirmed that even more flexible rods based on a 6HB design exhibit persistence lengths exceeding several hundred nanometers. Thus, the finding of unusually small values of the ratio ρ demands further investigation. In particular, we expect that lateral DNA single strands (handles, which are attached to the nano-rods to facilitate the attachment of nanoparticles or functional molecular moieties) affect the rotational and translational mobility and thus the apparent hydrodynamic radius, which in turn influences the shape sensitive ratio ρ. In addition, a reduction of the staple concentration in the folding mixture (as tested for 14HB in this study) may be acceptable with respect to achieving the proper shape of the DNA nanoparticles that is expected by design; nevertheless, missing staples might affect the compactness of the resulting nano-rod and thus its hydrodynamic mobility, as well. A systematic variation of all these parameters is beyond the scope of this preliminary study. Yet, further systematic investigations in this direction are expected to yield valuable additional insight. In conclusion, static light scattering and dynamic light scattering provide important tools for further basic studies on DNA origami nanostructures.

Acknowledgments

The authors are very grateful to Tim Liedl for his continuous support and encouragement, as well as his readiness to share his knowledge and his laboratory rooms and equipment. A scholarship for postdoctoral researchers by the President of Paderborn University is gratefully acknowledged.

Disclosure statement

No potential conflict of interest was reported by the authors.

Funding

This work was supported by a scholarship for postdoctoral researchers by the President of Paderborn University.

References

[1] A. Leforstier, and F. Livolant, *Liq. Cryst.* **17** (5), 651 (1994). DOI: 10.1080/02678299408037336
[2] M. Nakata *et al.*, *Science* **318** (5854), 1276 (2007). DOI: 10.1126/science.1143826
[3] K. Liu *et al.*, *Chem. Soc. Rev.* **46** (16), 5147 (2017). DOI: 10.1039/C7CS00165G
[4] M. Siavashpouri *et al.*, *Nat. Mater.* **16** (8), 849 (2017). DOI: 10.1038/nmat4909
[5] T. P. Fraccia *et al.*, *Orig. Life Evol. Biosph.* **45** (1-2), 51 (2015). DOI: 10.1007/s11084-015-9438-1
[6] Y. J. Cha *et al.*, *ACS Appl. Mater. Interfaces.* **7** (24), 13627 (2015). DOI: 10.1021/acsami.5b03321

[7] B. Zhang, J. Schmidtke, and H.-S. Kitzerow, *Adv. Optical Mater.* **7** (8), 1801766 (2019). DOI: 10.1002/adom.201801766
[8] K. Martens *et al.*, *Small* **12** (12), 1658 (2016). DOI: 10.1002/smll.201503382
[9] B. Atorf *et al.*, *Liq. Cryst.* **44** (12-13), 1 (2017). DOI: 10.1080/02678292.2017.1359692
[10] Q. Liu *et al.*, *Opt. Lett.* **44** (11), 2831 (2019). DOI: 10.1364/OL.44.002831
[11] P. Wang *et al.*, *Chem* **2** (3), 359 (2017). DOI: 10.1016/j.chempr.2017.02.009
[12] A. Kuzyk *et al.*, *ACS Photonics.* **5** (4), 1151 (2018). DOI: 10.1021/acsphotonics.7b01580
[13] S. Fan *et al.*, *Small* **15** (26), e1805554 (2019). DOI: 10.1002/smll.201805554
[14] A. Heuer-Jungemann, and T. Liedl, *Trends in Chemistry* **1** (9), 799 (2019). DOI: 10.1016/j.trechm.2019.07.006
[15] J. Dong, C. Zhou, and Q. Wang, *Top. Curr. Chem.* **378**, 33 (2020). DOI: 10.1007/s41061-020-0297-5
[16] K. Tapio, and I. Bald, *Multifunct. Mater.* **3** (3), 032001 (2020). DOI 10.1088/2399-7532/ab80d5
[17] P. W. K. Rothemund, *Nature* **440** (7082), 297 (2006). DOI: 10.1038/nature04586
[18] S. M. Douglas *et al.*, *Nature* **459** (7245), 414 (2009). DOI: 10.1038/nature08016
[19] W. Liu *et al.*, *Angew. Chem. Int. Ed. Engl.* **50** (1), 264 (2011). DOI: 10.1002/anie.201005911
[20] S. M. Douglas *et al.*, *Nucleic Acids Res.* **37** (15), 5001 (2009). DOI: 10.1093/nar/gkp436
[21] cadnano. https://cadnano.org
[22] C. E. Castro *et al.*, *Nat. Methods.* **8** (3), 221 (2011). DOI: 10.1038/nmeth.1570
[23] D. N. Kim *et al.*, *Nucleic Acids Res.* **40** (7), 2862 (2012). DOI: 10.1093/nar/gkr1173
[24] CanDo. https://cando-dna-origami.org
[25] S. Fischer *et al.*, *Nano Lett.* **16** (7), 4282 (2016). DOI: 10.1021/acs.nanolett.6b01335
[26] K. Xia *et al.*, *ACS Nano.* **14** (2), 1319 (2020). DOI: 10.1021/acsnano.9b09163
[27] B. Zhang *et al.*, *Nanomaterials* **10** (9), 1695 (2020). DOI: 10.3390/nano10091695
[28] M. F. Ober *et al.*, *Nat. Commun.* **13** (1), 5668 (2022). DOI: 10.1038/s41467-022-33083-5
[29] H. Ijäs *et al.*, *Biophys. J.* **121** (24), 4800 (2022). DOI: 10.1016/j.bpj.2022.10.036
[30] B. H. Zimm, *J. Chem. Phys* **16** (12), 1093 (1948). DOI: 10.1063/1.1746738
[31] Burchard, W. Static and dynamic light scattering from branched polymers and biopolymers. In *Light scattering from polymers. Advances in Polymer Science*, edited by W. Burchard (Springer-Verlag, Berlin), 1983, pp. 1–124.
[32] M. Schmidt, *Macromolecules* **17** (4), 553 (1984). DOI: 10.1021/ma00134a008
[33] Y. Xin *et al.*, *Small* **18** (18), e2107393 (2022). DOI: 10.1002/smll.202107393